Boosting visible light photocatalytic hydrogen evolution of graphitic carbon nitride via enhancing it interfacial redox activity with cobalt/nitrogen doped tubular graphitic carbon

Yanjie Si[a,b,1], Yijie Zhang[a,1], Luhua Lu[a,b,*], Si Zhang[a], Ying Chen[a,b], Jinghai Liu[c,*], Hongyun Jin[a], Shuen Hou[a], Kai Dai[d], Weiguo Song[e]

[a] Faculty of Materials Science and Chemistry, China University of Geosciences Wuhan, 388 Lumo Road, Wuhan 430074, PR China
[b] Zhejiang institute, China University of Geosciences Wuhan, Hangzhou, 311305, PR China
[c] Inner Mongolia Key Laboratory of Carbon Nanomaterials, College of Chemistry and Chemical Engineering, Inner Mongolia University for Nationalities, Tongliao, 028000, PR China
[d] College of Physics and Electronic Information, Huaibei Normal University, Huaibei, 235000, PR China
[e] Laboratory of Molecular Nanostructures and Nanotechnology, Institute of Chemistry, Chinese Academy of Sciences & Beijing National Laboratory of Molecular Sciences, Beijing, 100190, PR China

ARTICLE INFO

ABSTRACT

Carbon based nanomaterials have attracted great attentions in the fields of electrocatalysis and photocatalysis. Here, we report our recent progress on photocatalytic hydrogen evolution of graphitic carbon nitride (g-C_3N_4) by introducing carbon based electrocatalyst as co-catalyst. Cobalt/nitrogen doped graphitic carbon (Co-NG) composite with tubular structure was synthesized by cobalt catalyzed carbonization and graphitization of urea under thermal treatment. Co-NG with strong interaction of cobalt and nitrogen doped graphitic carbon has shown low overpotential for electrocatalytic hydrogen evolution reaction. It was thus used as co-catalyst for graphitic carbon nitride (g-C_3N_4). Beside enhanced light absorption and reduced recombination of Co-NG/g-C_3N_4 heterostructure composite, high interfacial redox reaction activity of Co-NG was found. The photocatalytic hydrogen evolution activity of Co-NG/g-C_3N_4 was thus effectively improved.

1. Introduction

Molecular hydrogen has been worldwide recognized as sustainable clean energy carrier [1]. Scalable production of hydrogen at low cost via environmental compatible approaches is eagerly desired. To achieve this goal, varieties of technologies such as electrocatalytic hydrogen evolution and photocatalytic hydrogen evolution have been developed [2–4].

The most promising catalysts for electrocatalytic hydrogen evolution are Pt based materials [5]. However, highly use of Pt has largely limited scale application of electrocatalytic technology. None-noble metal catalysts such as metal sulphides, nitrides and phosphorous were developed recent years [6–11]. In compared with these catalysts, low cost carbon based materials were found to have stable catalytic activity for long-run hydrogen evolution reaction (HER) [12,13]. Very recent research have found that carbon materials composited with low concentration transitional metals have displayed HER activity comparable

to variety of transitional metals based compounds for the tuned hydrogen adsorption/desorption free energy of catalysts with strong interaction of finely dispersed metal atoms with carbon materials surface [14,15].

Beside electrocatalytic hydrogen evolution, photocatalytic hydrogen evolution (PHE) based on semiconducting materials has also been developed for its advance in direct transition of solar energy to chemical energy without extra electrical energy consumption [16]. In compared with other transitional metal based semiconducting materials, graphitic carbon nitride (g-C_3N_4) with low expense for scalable production, narrow band-gap for visible light photocatalysis, stable structure and environmental compatibility was regard as green candidate for PHE [17]. However, PHE activity of it is much lower than other transitional metal based compounds even when photo-generated electrons in pristine g-C_3N_4 possess thermodynamically sufficient potential for hydrogen evolution [18]. Very recent research has point out that photo-generated electron, which is deep trapped in g-C_3N_4 and has no

---

reactivity for reduction of proton, would severely impede accumulation of holes necessary for multi-hole water oxidation and thus depress hydrogen evolution for full water splitting [19]. During photocatalytic process, hole reaction would be limited if the electron reaction rate is low and vice visa [20]. Since effective PHE requires catalysts with surface of low hydrogen evolution potential, scalable productive and highly active interfacial materials are thus of great value for advancing PHE activity of catalysts [21]. Recent researches have shown that beside enhanced charge separation effect, co-catalysts have played important on accelerating g-C_3N_4 interfacial charge transfer for improving its PHE activity [22–28]. Wang has shown that depositing CoP and Pt on g-C_3N_4 can effective enhance its interfacial oxidation and reduction overpotential respectively and thus higher hydrogen evolution rate under visible light can be achieved [29].

Inspired by these recent researches, we have synthesized a cobalt/nitrogen doped graphitic carbon (Co-NG) composite by cobalt catalyzed carbonization and graphitization of urea under thermal treatment. EXAFS spectra along with XPS analysis of Co-NG have confirmed the strong coordination of cobalt atoms with nitrogen doped graphitic carbon, which was regarded to be important for achieving high HER activity. Co-NG with promising electrocatalytic hydrogen evolution reaction (HER) activity has shown over potential of 203 mV at 10 mA cm^{-2} current density in 0.5 M H_2SO_4 solution. By compositing Co-NG with g-C_3N_4 via sonication treatment, effective improved PHE activity has been achieved. Co-NG/g-C_3N_4 has displayed PHE rate of 2.5 times than that of g-C_3N_4. The apparent quantum efficiency under 420 nm monochromatic light irradiation of it was found to be 12.75%. Electrochemical and photophysical analysis were used to probe origin of enhanced PHE activity. Beside enhanced light absorption and reduced recombination of photo-generated electrons and holes in Co-NG/g-C_3N_4 with tuned photonic properties, Co-NG on the surface of g-C_3N_4 has effectively reduced electron and hole reaction overpotential of Co-NG/g-C_3N_4 composite. The enhanced interfacial redox reaction ability of Co-NG/g-C_3N_4 by introduced Co-NG benefits electron/hole-transfer reaction. The improved interfacial reduction activity of electron along with that of hole together leads to depressed recombination of them during PHE process and thus has promoted its PHE activity.

2. Experimental section

2.1. Preparation

To prepare Co-NG, 10 g urea was mixed with 1 g $Co(Ac)_2$ in 50 mL deionized water under stirring for 30 min and then freeze dried to remove water. The mixture was grid and placed in a covered corundum crucible and heated to desired temperature (700, 800 or 900 °C) with temperature increase rate of 10 °Cmin^{-1} and preserved for 2 h. The obtained sample was named Co-NG-X while X represent temperature. The collected sample was them washed by 100 mL 1 M HCl acid for three times to remove acid soluble cobalt. The final product was named Co-NG-X-A. To prepare g-C_3N_4, 10 g urea (AR, Sinopharm Chemical Reagent Co., Ltd) was placed in a covered corundum crucible and heated to 550 °C with temperature increase rate of 10 °C min^{-1} and preserved for 3 h in air atmosphere and naturally cooled to room temperature in a tube furnace. Pt loaded Co-NG-X-A/g-C_3N_4 (or g-C_3N_4) was obtained by photo-deposition. 0.3 mL $H_2PtCl_6\cdot6H_2O$ (10 mg/mL, AR, Sinopharm Chemical Reagent Co., Ltd) and 2 mL acetic acid (1 mol L^{-1}, Sinopharm Chemical Reagent Co., Ltd) were added into 100 mL Co-NG-X-A/g-C_3N_4 dispersion (1 mg mL^{-1}) to obtain 3 wt% Pt-Co-NG-X-A/g-C_3N_4 (or Pt-g-C_3N_4). After N_2 bubbling for an hour to remove the oxygen (O_2) in the system, the sample was irradiated by a 300 W Xe lamp (PLS-SXE 300, Beijing Perfect light Technology Co., Ltd) for three hours. Then, the Pt-g-C_3N_4 (or Pt-Co-NG-X-A/g-C_3N_4) was obtained by filtering and drying at 80 °C.

2.2. Characterization

All measurement was carried out in 25 °C room temperature environment. Morphology of samples was characterized through SEM (HITACH S-4800) and TEM (Tecnai G2 F20S-TWIN at 200 kV). Structure analysis was carried out through XRD (Bruker AXS D8-Focus) and XPS (X'Pert-Pro MPD using Cu Kα (λ = 1.5406 A). UV–vis DRS measurements were carried out using a Hitachi UV-3600 UV–vis spectrophotometer equipped with an integrating sphere attachment. Analysis range was from 200 to 600 nm, and $BaSO_4$ was used as a reflectance standard. PL spectra of photocatalysts were measured by FLS920 with excitation wavelength of 325 nm.

2.3. Electrocatalytic measurement

Electrochemical measurements were carried out on a CHI760E electrochemical work station (Shanghai Chenhua) in three electrodes system. To remove bubbles generated during measurement, rotation speed of electrode has been controlled 1600 rpm by MRS electrode rotator (Pine Research Instrumentation, USA). Typically, 1 mg of catalyst and 10 μL of 5 wt% Nafion solution were dispersed in 1 mL of 6:1(v/v) water/ethanol and sonication for 2 h to form a homogenous solution. 60 μL solution was loaded on a 5-mm-diamter clean glassy carbon rotation disk electrode (mass loading ～0.3 mg cm^{-2}) and dried under room temperature. Measurement was carried out in 0.5 M H_2SO_4 or 10% TEOA solution, with a Pt wire as counter electrode and reference electrode was Ag/AgCl. LSV measurement was scanned at scan rate of 2 mV s^{-1}. Before measurement, electrolyte solution was bubbled with N_2 and H_2 for 1 h to completely remove O_2 and scanned CV until a stable curve is achieved.

2.4. Photocatalytic measurement

Photocatalytic water splitting reactions were carried out in a Pyrex top-irradiation reaction vessel connected to a glass closed gas circulation system. 80 mg Pt loaded catalyst was dispersed in a mixture of 50 mL deionized water and 6 mL triethanolamine (TEOA) (78%, Sinopharm Chemical Reagent Co., Ltd) by sonication for 0.5 h. The obtained reactant dispersion was put into reaction vessel and stirred. Reaction system was evacuated three times with half an hour each time to remove air completely prior to irradiation under a 300 W Xe lamp with water filter. Wavelength of incident light was controlled by using cut-off filters (> 400 nm). For apparent quantum efficiency calculation, band pass filter of 420 nm was used. The light intensity was measured by PL-MW2000. The temperature of reactant solution was maintained at room temperature by a flow of cooling water during reaction. Evolved gases were analyzed by gas chromatography (GC 7890II, Shanghai Techcomp Instrument Ltd.) equipped with a thermal conductive detector (TCD) with argon as carrier gas.

3. Results and discussion

Morphology of Co-NG-700-A, Co-NG-800-A and Co-NG-900-A can be seen from scanning electron microscope (SEM) images. Co-NG-700-A and Co-NG-800-A have shown typical tubular morphology. When thermal treatment temperature increased to 900 °C, large amount of carbon spheres were formed. Transmission electron microscope (TEM) image (Fig. 1D) has shown typical bamboo like tubular carbon of Co-NG-800-A with small amount of residual cobalt particle wrapped by graphitic carbon layers. Moreover, high resolution TEM (HR-TEM) image in Fig. 1E has shown very small cobalt atom clusters (less than 1 nm) were dispersed between graphitic carbon layers. High-angle annular dark-field scanning transmission electron microscope (HAADF-STEM) image (Fig. 1E) and element mapping (Fig. 1F, G and H) have revealed the existence of doped nitrogen and cobalt particles.

XRD analysis in Fig. 2 has shown largely enhanced peak intensity at
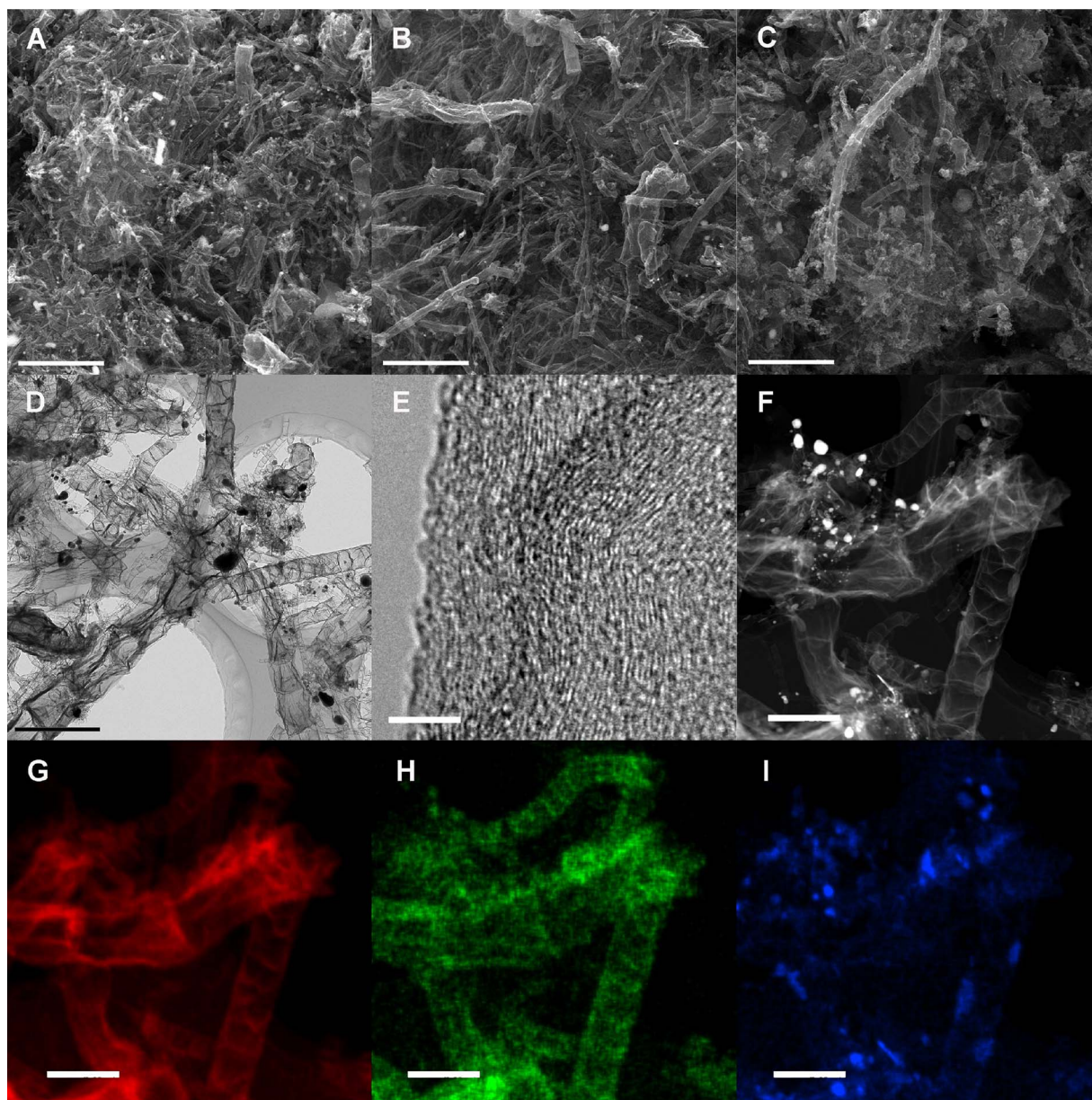
Fig. 1. SEM images for (A) Co-NG-700-A, scale bar 5 μm, (B) Co-NG-800-A, scale bar 5 μm and (C) Co-NG-900-A, scale bar 5 μm, (D) TEM image for Co-NG-800-A, scale bar 200 nm, (E) HR-TEM image for Co-NG-800-A, scale bar 5 nm, (F) HAADF-STEM image and elemental mappings of (G) Carbon, (H) Nitrogen and (I) cobalt for Co-NG-800-A, scale bar 200 nm.
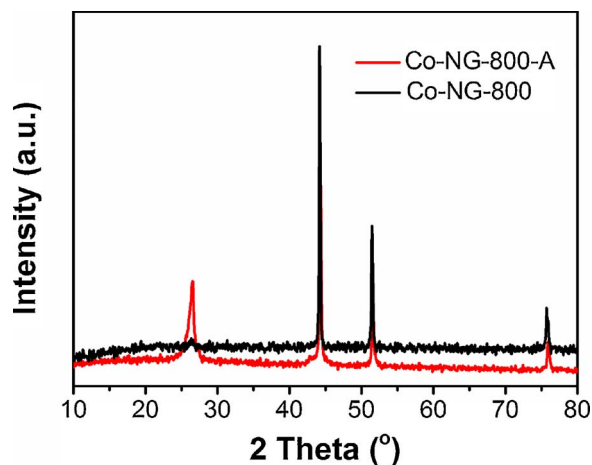

Fig. 2. XRD patterns of Co-NG-800 and Co-NG-800-A respectively.

26.4° for 002 facet of graphitic carbon in Co-NG-800-A after acid washing Co-NG-800 to remove soluble cobalt particles, which further confirmed existence of graphitic layer structure of Co-NG-800-A. The formation of graphitic structure of carbon was attributed to catalytic growth of carbon by cobalt [30,31].

To investigate bond states of cobalt, Fourier transformed k^3-weighted EXAFS spectra in R space at the Co K-e−e for Co-NG-800-A in compared with metallic cobalt foil and cobalt oxides has been shown in Fig. 3A. One broad peak with path length of 1.19 Å and a strong peak with path length of 1.94 Å were found. The path length of 1.19 Å is lower than 1.42 Å of Co−O for Co_3O_4 but close to that of Co−N and Co−C bonds [32–34]. The path length of 1.94 Å is close to that of Co−Co bond of Co_xC (1.93 Å) [34]. Result indicates that small cobalt nanoparticles or clusters imbedded in nitrogen doped graphene have strong interaction with carbon and nitrogen atoms. For comparison, X-ray photoelectron spectroscopy (XPS) analysis was carried out. Deconvoluted $Co2p_{3/2}$ spectrum (Fig. 3B) has shown peaks of Co^0 (777.9 eV) [35–38], Co−C (778.8 eV) [39], Co^{2+} (779.9 eV) for CoO [40] and Co-N (781.1 eV) [36,37], in well accordance with that of

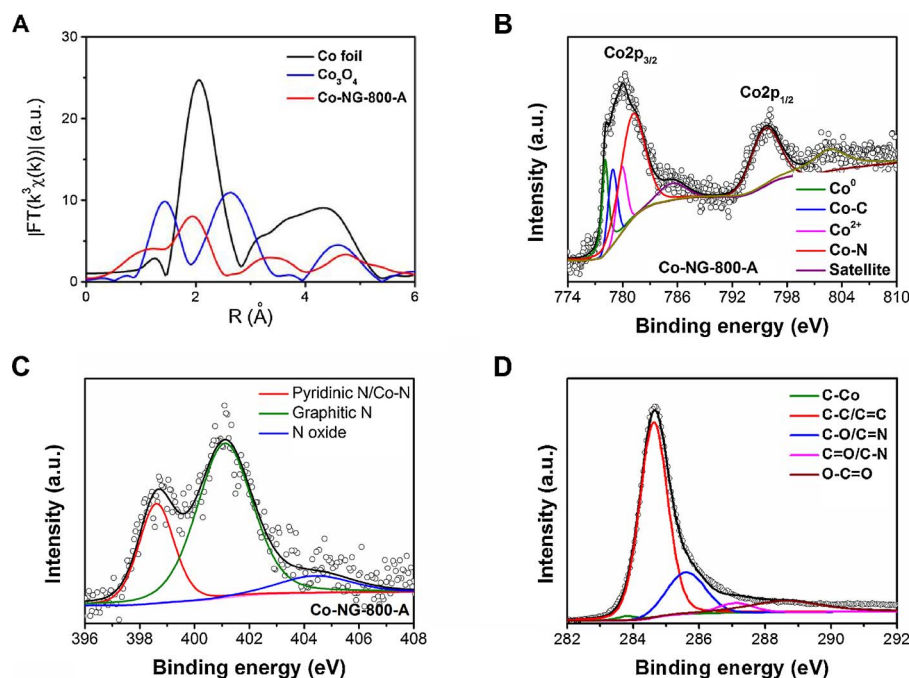**Fig. 3.** (A) Fourier transformed k³-weighted EXAFS spectra in R space and Deconvoluted (B) Co2p, (C) N1 s and (D) C1 s XPS spectrums of Co-NG-800-A.

EXAFS spectra analysis. Deconvoluted N1 s spectrum in Fig. 3C has shown peaks of N—Co and pyridinic N (398.4 eV), graphitic N (401.2 eV) and N-oxide (404.1 eV) [35]. Since peaks of N—Co and pyridinic N are very close [14,35], they are hard to be further deconvoluted from N1 s XPS spectrum. Deconvoluted C1 s spectrum in Fig. 3D has shown peaks of C—Co (283.9 eV) bond [40,41] along with C—C/C=C (284.6 eV), C—O/C=N (285.7 eV), C=O/C—N (287.1 eV) and O—C=O (288.6 eV) bonds for Co-NG-800-A.

LSV curves for Co-NG-X-A synthesized under different temperature have been shown in Fig. 4A. The onset potential of Co-NG-700-A, Co-NG-800-A and Co-NG-900-A were found to be 30, 40, and 48 mV respectively. Under current density of 10 mA cm⁻² the overpotential of Co-NG-700-A, Co-NG-800-A and Co-NG-900-A were found to be 286, 203 and 236 mV respectively. We can see that Co-NG-800-A has

displayed highest HER activity in compared with other samples. Via XPS analysis, it was found that higher synthetic temperature results in lower nitrogen doping content (Table S1) especially that of pyridinic nitrogen (Fig. S1) while lower temperature results in poor chemical bonding of cobalt with nitrogen (Fig. S2). Since effective coordination of cobalt with sufficient doped nitrogen can effective tuning hydrogen adsorption/desorption energy on active carbon atoms that bonded with cobalt coordinated nitrogen (formation of Co-N—C active sites) [14,15], and thus reduced active sites for electrocatalytic HER of those sample should be attributed to insufficient chemical bonding of cobalt with pyridinic nitrogen in Co-NG-700-A and Co-NG-900-A. To study kinetics of HER processes, Tafel plots of catalysts have been transferred from LSV curves and have been shown in Fig. 4B. It was known that hydrogen evolution in acid solutions involves three major reactions [35].
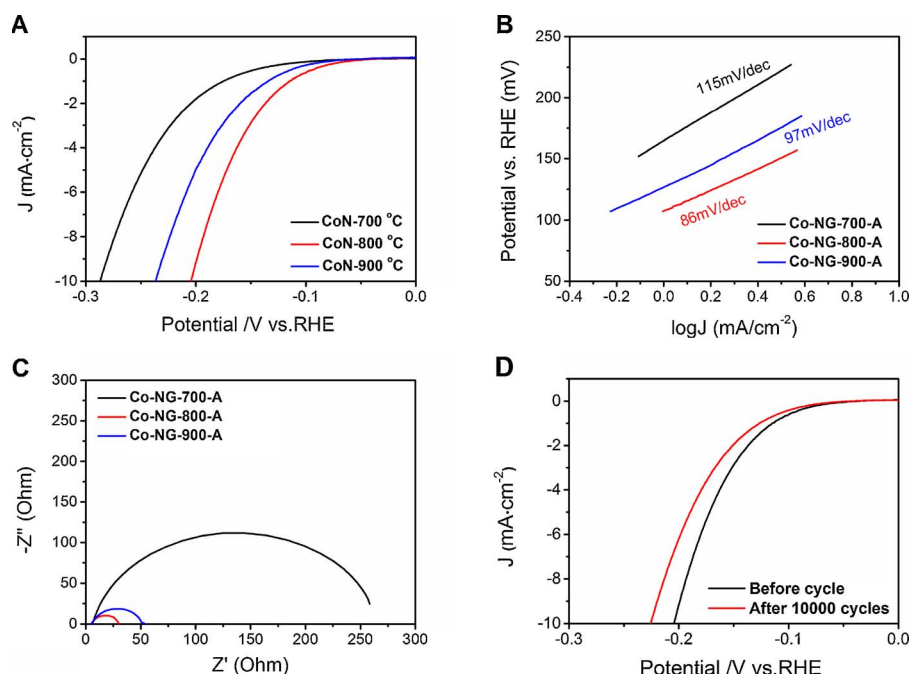

Fig. 4. (A) LSV curves and corresponding (B) Tafel plots obtained in 0.5 M H₂SO₄ at 2 mV·s⁻¹, (C) Nyquist plots measured at −0.4 V vs RHE for samples, (D) Cyclic stability of Co-NG-800-A in 0.5 M H₂SO₄ solution.

The Volmer reaction with a Tafel slope of $120\,mV\,dec^{-1}$ represents primary discharge step. Heyrovsky reaction with a Tafel slope of $40\,mV\,dec^{-1}$ represents electrochemical desorption step. Tafel reaction with a Tafel slope of $30\,mV\,dec^{-1}$ represents a combination step of adsorbed hydrogen on catalysts. Co-NG-800-A has a Tafel slope of $86\,mV\,dec^{-1}$, much lower than that of other samples. By comparing these data, we can deduct that Co-NG-800-A follows the Heyrovsky step. Hydrogen evolution requires faradic charge transfer reaction, the feasibility of which can be reflected by charge transfer resistance (R_{ct}) of catalysts. Electrochemical impedance spectroscopy (EIS) results in Fig. 4C have shown that R_{ct} of Co-NG-700-A, Co-NG-800-A and Co-NG-900-A were found to be 258, 25 and 46 ohm respectively. In accordance with LSV analysis, Co-NG-800-A has shown smallest R_{ct} indicating feasibility of HER on active sites of Co-NG-800-A. Moreover, cyclic stability of Co-NG-800-A in acidic solution was found to be good as has been shown in Fig. 4D.

As has been discussed above, enhancing interfacial redox activity of photocatalysts is crucially important for achieving high photocatalytic hydrogen evolution (PHE) activity. Thus, Co-NG-800-A was composited with g-C$_3$N$_4$ via sonication treatment. The typical morphology of pure g-C$_3$N$_4$ can be seen in Fig. 5A. Large scale scanning electron microscope (SEM) images of g-C$_3$N$_4$ (Fig. S3) has further conformed uniform morphology of it. XRD pattern (Fig. S4) of g-C$_3$N$_4$ has shown layered structure of it with two peaks centered at 12.8° and 27.4° for typical 100 and 002 facets of it [18]. After compositing, bamboo-like Co-NG-800-A can be seen in TEM image (Fig. 5B) of their composite (named Co-NG/g-C$_3$N$_4$). Since Co-NG and g-C$_3$N$_4$ are both carbon materials, it is hard to distinguish them by morphology. Element mapping was carried out to get more information. The selected area in Fig. 5B was once imaged via dark field scanning TEM as has been shown in Fig. 5C. The element mapping images of carbon, nitrogen and cobalt of selected area have been shown in Fig. 5D, E and F. As can be seen in Fig. 5D, the contrast of mapping image for carbon of Co-NG is slightly higher than g-C$_3$N$_4$ for

its higher concentration of carbon in Co-NG. Co-NG has poor nitrogen element concentration in compared with that of g-C$_3$N$_4$. Thus the element mapping of nitrogen (Fig. 5E) has clearly distinguished Co-NG from g-C$_3$N$_4$. Accordingly, enriched cobalt in Co-NG (Fig. 5F) has further distinguished Co-NG from g-C$_3$N$_4$.

PHE for Co-NG/g-C$_3$N$_4$ with different Co-NG weight fraction and 3% weight percent of loaded Pt along with triethanolamine (TEOA) as sacrificial donors was online measured under visible light irradiation and has been shown in Fig. 6A. It can been see that highest hydrogen evolution of $6227\,\mu mol\,g^{-1}$ was achieved by 0.05%Co-NG/g-C$_3$N$_4$ with 0.05% weight percent of Co-NG after 3.1 h visible light irradiation in compared with 2511, 4302, 4944 and $2656\,\mu mol\,g^{-1}$ of g-C$_3$N$_4$, 0.02%Co-NG/g-C$_3$N$_4$, 0.07%Co-NG/g-C$_3$N$_4$ and 0.5%Co-NG/g-C$_3$N$_4$. The calculated PHE rate for Co-NG/g-C$_3$N$_4$ under visible light irradiation was found to be $2009\,\mu mol\,g^{-1}\,h^{-1}$, which is 2.5 times of g-C$_3$N$_4$ as has been shown in Fig. 6B. Besides, PHE activity of 0.05%Co-NG/g-C$_3$N$_4$ and g-C$_3$N$_4$ without loading Pt under visible light irradiation has also been measured (Fig. S5). Lack of Pt as hydrogen evolution active site would reduce PHE yield for both 0.05%Co-NG/g-C$_3$N$_4$ and g-C$_3$N$_4$. But 0.05%Co-NG/g-C$_3$N$_4$ still displayed higher PHE yield than g-C$_3$N$_4$, indicating Co-NG has contribution to PHE process. Since apparent quantum efficiency of catalysts is important for evaluate their PHE activity, we have measured PHE activity and calculated apparent quantum efficiencies of catalysts with 3% loaded Pt under 420 nm monochromatic light irradiation for comparison as have been shown in Fig. 6C. The calculated apparent quantum efficiencies of g-C$_3$N$_4$, 0.02%Co-NG/g-C$_3$N$_4$, 0.05%Co-NG/g-C$_3$N$_4$, 0.07%Co-NG/g-C$_3$N$_4$ and 0.5%Co-NG/g-C$_3$N$_4$ were found to be 4.51%, 10.08%, 12.75%, 10.17% and 5.14% respectively (See Table S2). It has indicated that proper amount of Co-NG as co-catalyst has effectively enhanced PHE activity of g-C$_3$N$_4$. Moreover, cyclic test (Fig. 6D) has shown good stability of 0.05%Co-NG/g-C$_3$N$_4$. The according SEM images and XRD patterns of 0.05%Co-NG/g-C$_3$N$_4$ before and after PHE test have shown no obvious
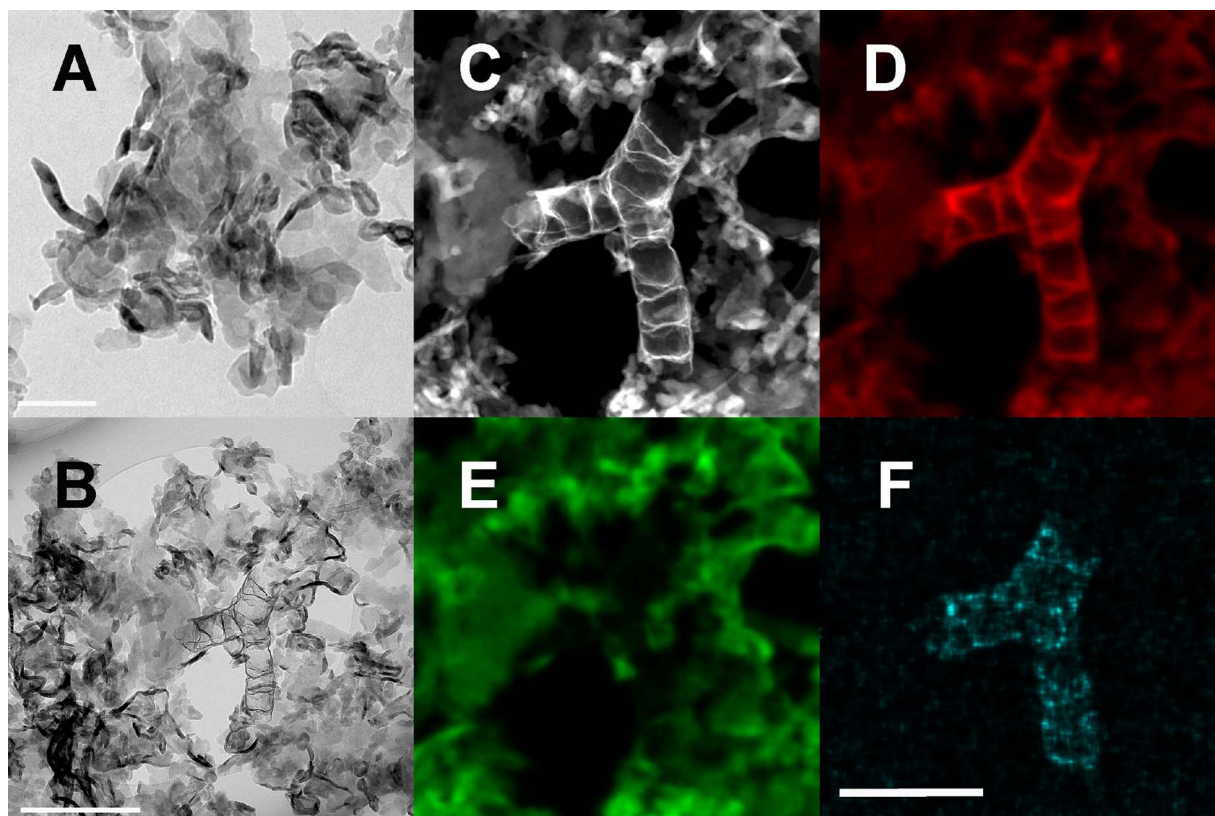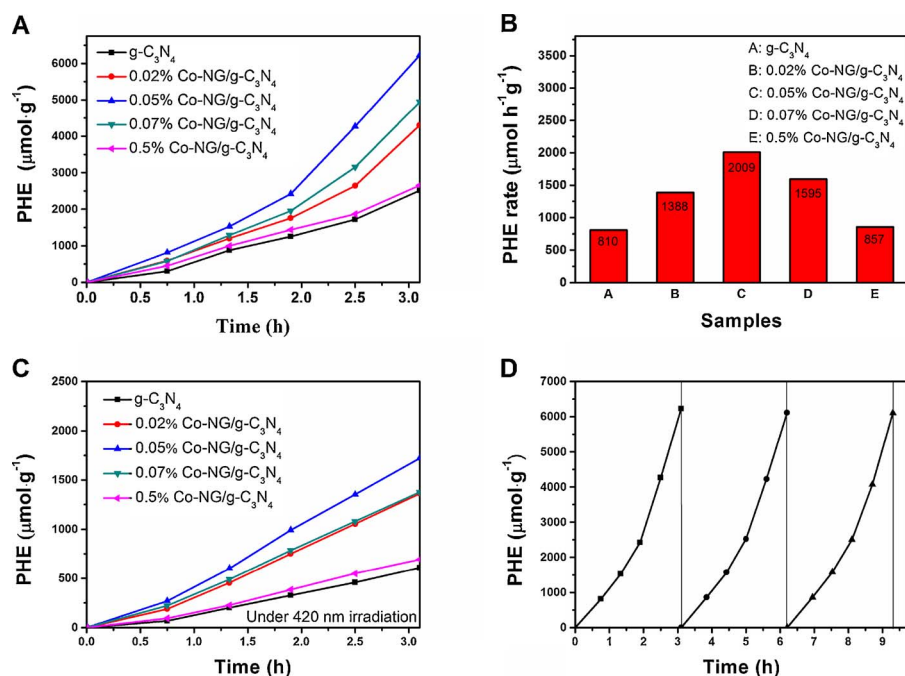

Fig. 5. (A) TEM image of g-C$_3$N$_4$, scale bar 200 nm, (B) Co-NG/g-C$_3$N$_4$, scale bar 500 nm, (C) HAADF-STEM image and elemental mappings of (D) Carbon, (E) Nitrogen and (F) cobalt for Co-NG-800-A, scale bar 200 nm.

Fig. 6. (A) PHE under visible light irradiation, (B) comparison of PHE rate and (C) PHE under 420 nm monochromatic light irradiation (achieved via 420 nm band pass filter) for catalysts loaded with 3% Pt, (D) cyclic stability under visible light irradiation for 0.05%Co-NG/g-C_3N_4 loaded with 3% Pt.

morphology and structure change (Fig. S6).

To investigate the role of Co-NG on PHE activity for g-C_3N_4, photophysical and electrochemical properties of Co-NG/g-C_3N_4 in compared with g-C_3N_4 have been characterized. UV–vis DRS spectrums in Fig. 7A has shown that introducing Co-NG has not changed the bandgap of g-C_3N_4. Photoluminescence spectrums in Fig. 7B have shown that increasing weight fraction of Co-NG in the composite has reduced intensity of photoluminescence indicating reduced recombination of photo-generated electrons and holes. This is in accordance with previously published work on carbon/g-C_3N_4 based PHE catalysts [42–44]. Recent research have shown that interfacial redox activity enhancement is crucially important for boosting hydrogen evolution activity of g-C_3N_4 [45–47]. Thus, we have investigated interfacial redox activity of composites in the same TEOA solution environment condition for PHE by electrochemical analysis. Result in Fig. 7C exhibits overpotential (vs

Ag/AgCl) for interfacial reduction reaction under current density of 0.5 mAcm^{-2} reduces as weight fraction of Co-NG increases. The oxidation reaction current on interface of composites in Fig. 7D increases as weight fraction of Co-NG increases. Electrochemical analysis has indicated important role of Co-NG on promoting electron and hole reaction for PHE. These results has first time proved that carbon materials on the surface of g-C_3N_4 depress electron and hole recombination via enhanced electron and hole interfacial reaction activity, which facilitates reduction of H_2O to H_2 for PHE.

As has been analysis above, charge separation and interfacial redox activity of Co-NG/g-C_3N_4 composites increase as weight fraction of Co-NG-800-A increases. However, the PHE activity of Co-NG/g-C_3N_4 does not follow this trend and has an optimal value for 0.05%Co-NG/g-C_3N_4. Photocurrent measurement has been carried out to study their ability of generated electrons under visible light irradiation. As has been shown
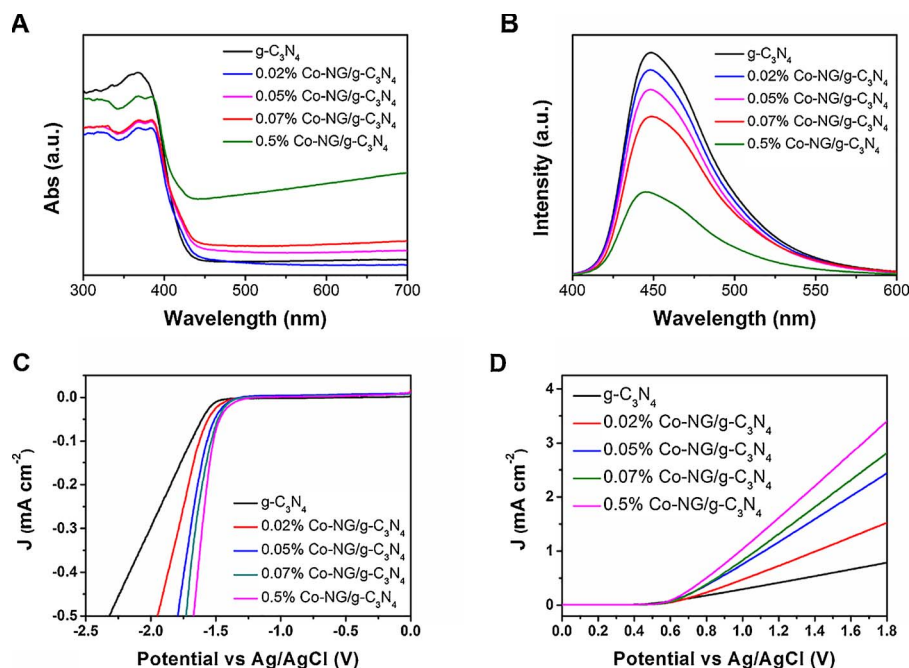
Fig. 7. (A) UV–vis DRS spectrums, (B) Photoluminescence spectrums, (C) LSV curves of a cathodic scan from 0 to −2.3 V (vs Ag/AgCl) in TEOA solution, (D) LSV curves of an anodic scan from 0 to 1.8 V (vs Ag/AgCl) in TEOA solution for Co-NG/g-C_3N_4 and g-C_3N_4 samples.
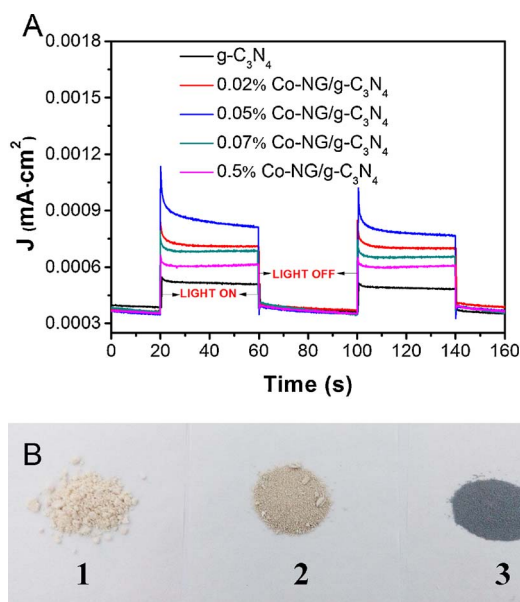
Fig. 8. (A) Photo-current measurement of catalysts in 0.5 M Na$_2$SO$_4$ solution under 0.5 V (vs Ag/AgCl), (B) Photo of catalysts powder for (1) g-C$_3$N$_4$, (2) 0.05%Co-NG/g-C$_3$N$_4$ and (3) 0.5%Co-NG/g-C$_3$N$_4$ respectively.

in Fig. 8A, 0.05%Co-NG/g-C$_3$N$_4$ displayed highest photocurrent. It should be noticed that light absorption by carbon materials with zero band-gap do not generating electron/hole pairs within them. In Fig. 8B we can see that 0.5%Co-NG/g-C$_3$N$_4$ has become black powder, indicating too much Co-NG on g-C$_3$N$_4$ surface would prevent light absorption by g-C$_3$N$_4$ and reduce effective electron/hole generation for PHE. Thus, a compromise among light absorption, charge separation and surface redox activity for the optimal PHE activity is achieved by 0.05%Co-NG/g-C$_3$N$_4$.

4. Conclusions

In conclusion, we have synthesized Co-NG composites with tubular graphitic carbon morphology by cobalt catalyzed carbonization and graphitization of urea under thermal treatment. The composite synthesized under 800 °C has shown low overpotential for electrocatalytic hydrogen evolution reaction, which is an important character of potential co-catalyst for photocatalytic hydrogen evolution. It was thus used to boost photocatalytic hydrogen evolution of g-C$_3$N$_4$. Beside extended light absorption and reduced recombination of photo-generated electrons and holes of cobalt/nitrogen doped graphitic carbon/g-C$_3$N$_4$ composite, cobalt/nitrogen doped graphitic carbon was found to have reduced overpotential for redox reaction on the interface of g-C$_3$N$_4$, which improved electron and hole reactivity towards interfacial redox and thus effective enhanced photocatalytic hydrogen evolution activity of g-C$_3$N$_4$.

Acknowledgements

Appendix A. Supplementary data

Supplementary data associated with this article can be found, in the online version, at https://doi.org/10.1016/j.apcatb.2017.12.010.

References

[1] I.E.L. Stephens, J. Rossmeisl, I. Chorkendorff, Science 354 (2016) 1378–1379.
[2] D. Deng, K.S. Novoselov, Q. Fu, N. Zheng, Z. Tian, X. Bao, Nat. Nanotech. 11 (2016) 218–230.
[3] Q. Xiang, B. Cheng, J. Yu, Angew. Chem. Int. Ed. 54 (2015) 11350–11366.
[4] M. Titirici, R.J. White, N. Brun, V.L. Budarin, D.S. Su, F. Monte, J.H. Clark, M.J. MacLachlan, Chem. Soc. Rev. 44 (2015) 250–290.
[5] Y. Xu, B. Zhang, Chem. Soc. Rev. 43 (2014) 2439–2450.
[6] M.Y. Gao, C. Yang, Q.B. Zhang, J.R. Zeng, X.T. Li, Y.X. Hua, C.Y. Xu, P. Dong, J. Mater. Chem. A 5 (2017) 5797–5805.
[7] Y.P. Liu, Q.J. Li, R. Si, G.D. Li, W. Li, D.P. Liu, D.J. Wang, L. Sun, Y. Zhang, X.X. Zou, Adv. Mater. 29 (2017) 1606200.
[8] C.B. Lu, D. Tranca, J. Zhang, F. RodríguezHernández, Y.Z. Su, X.D. Zhuang, F. Zhang, G. Seifert, X.L. Feng, ACS Nano 11 (2017) 3933–3942.
[9] B. Zhang, C.H. Xiao, S.M. Xie, J. Liang, X. Chen, Y.H. Tang, Chem. Mater. 28 (2016) 6934–6941.
[10] Y.W. Tan, H. Wang, P. Liu, Y.H. Shen, C. Cheng, A. Hirata, T. Fujita, Z. Tang, M.W. Chen, Energy Environ. Sci. 9 (2016) 2257–2261.
[11] B. Bayatsarmadi, Y. Zheng, V. Russo, L. Ge, C.S. Casari, S.Z. Qiao, Nanoscale 8 (2016) 18507–18515.
[12] J. Duan, S. Chen, M. Jaroniec, S.Z. Qiao, ACS Catal. 5 (2015) 5207–5234.
[13] W. Zhou, J. Jia, J. Lu, L. Yang, D. Hou, G. Li, S. Chen, Nano Energy 28 (2016) 29–43.
[14] H.L. Fei, J.C. Dong, M.J. Arellano-Jiménez, G.L. Ye, N.D. Kim, E.L. Samuel, Z.W. Peng, Z. Zhu, F. Qin, J.M. Bao, M.J. Yacaman, P.M. Ajayan, D.L. Chen, Nat. Commun. 6 (2015) 8668.
[15] H.W. Liang, S. Brüller, R.H. Dong, J. Zhang, X.L. Feng, K. Müllen, Nat. Commun. 6 (2015) 7992.
[16] N.S. Lewis, Science 351 (2016) (aad1920).
[17] Y. Zheng, L. Jin, B. Wang, X. Wang, Angew. Chem. Int. Ed. 54 (2015) 12868–12884.
[18] S. Cao, J. Low, J. Yu, M. Jaroniec, Adv. Mater. 27 (2015) 2150–2176.
[19] R. Godin, Y. Wang, M.A. Zwijnenburg, J. Tang, J.R. Durrant, J. Am. Chem. Soc. 139 (2017) 5216–5224.
[20] P.V. Kamat, Acc. Chem. Res. 50 (2017) 527–531.
[21] J. Yang, D. Wang, H. Han, C. Li, Acc. Chem. Res. 46 (2013) 1900–1909.
[22] E.J. Popczun, C.G. Read, C.W. Roske, N.S. Lewis, R.E. Schaak, Angew. Chem. Int. Ed. 126 (2014) 5531–5534.
[23] J. Ryu, N. Jung, J.H. Jang, H. Kim, S.J. Yoo, ACS Catal. 5 (2015) 4066–4074.
[24] H. Zhao, J. Wang, Y. Dong, P. Jiang, ACS Sustainable Chem. Eng. 5 (2017) 8053–8060.
[25] Y. Hou, Y. Zhu, Y. Xu, X. Wang, Appl. Catal. B: Environ. 156–157 (2014) 122–127.
[26] D. Zeng, W. Ong, H. Zheng, M. Wu, Y. Chen, D. Peng, M. Han, J. Mater. Chem. A 5 (2017) 16171–16178.
[27] C. Li, Y. Du, D. Wang, S. Yin, W. Tu, Z. Chen, M. Kraft, G. Chen, R. Xu, Adv. Funct. Mater. 27 (2017) 1604328.
[28] L. Bi, X. Gao, L. Zhang, D. Wang, X. Zou, T. Xie, ChemSusChem (2017), http://dx.doi.org/10.1002/cssc.201701574.
[29] Z. Pan, Y. Zheng, F. Guo, P. Niu, X. Wang, ChemSusChem 10 (2016) 87–90.
[30] R.W. Fu, T.F. Baumann, S. Cronin, G. Dresselhaus, M.S. Dresselhaus, J.H. Satcher, Langmuir 21 (2005) 2647–2651.
[31] H. Ago, Y. Ito, N. Mizuta, K. Yoshida, B.S. Hu, C.M. Orofeo, M. Tsuji, K. Ikeda, S. Mizuno, ACS Nano 4 (2010) 7407–7414.
[32] P. Yin, T. Yao, Y. Wu, L. Zheng, Y. Lin, W. Liu, J. Ju, X. Hong, Z. Deng, G. Zhou, S. Wei, Y. Li, Angew. Chem. Int. Ed. 55 (2016) 10800–10805.
[33] Y. Tong, P.Z. Chen, T.P. Zhou, K. Xu, W.S. Chu, C.Z. Wu, Y. Xie, Angew. Chem. Int. Ed. 56 (2017) 7121–7125.
[34] G. Kwak, M.H. Woo, S.C. Kang, H.G. Park, Y.J. Lee, K.W. Jun, K.S. Ha, J. Catal. 307 (2013) 27–36.
[35] H. Zhang, Z. Ma, J. Duan, H. Liu, G. Liu, T. Wang, K. Chang, M. Li, L. Shi, X. Meng, K. Wu, J. Ye, ACS Nano 10 (2015) 684–694.
[36] Z. Yao, A. Zhu, J. Chen, X. Wang, C.T. Au, C. Shi, J. Solid State Chem. 180 (2007) 2635–2640.
[37] Z. Yao, A. Zhang, Y. Li, Y. Zhang, X. Cheng, C. Shi, J. Alloys Compd. 464 (2008) 488–496.
[38] L.E. Klebanoff, D.G. Van Campen, R.J. Pouliot, Phys. Rev. B 49 (1994) 2047–2057.
[39] A. Kong, Q. Lin, C. Mao, X. Bu, P. Feng, Chem. Commun. 50 (2014) 15619–15622.
[40] K. Hada, M. Nagai, S. Omi, J. Phys. Chem. B 105 (2001) 4084–4093.
[41] J. Xiong, Y. Ding, T. Wang, L. Yan, W. Chen, H. Zhu, Y. Lu, Catal. Lett. 102 (2005) 3–4.
[42] W. Ong, L. Tan, S. Chai, S. Yong, A.R. Mohamed, Nano Energy 13 (2015) 757–770.
[43] Q. Xu, C. Jiang, B. Cheng, J. Yu, Dalton Trans. (2017), http://dx.doi.org/10.1039/C7DT00629B.
[44] M.Z. Rahman, J. Zhang, Y. Tang, K. Davey, S. Qiao, Mater. Chem. Front. 1 (2017) 562–571.
[45] G. Zhang, Z. Lan, L. Lin, S. Lin, X. Wang, Chem. Sci. 7 (2016) 3062–3066.
[46] C.A. Caputo, M.A. Gross, V.W. Lau, C. Cavazza, B.V. Lotsch, E. Reisner, Angew. Chem. Int. Ed. 53 (2014) 11538–11542.
[47] G. Zhang, Z. Lan, X. Wang, Chem. Sci. 8 (2017) 5261–5274.